Time-frequency analysis of acceleration data from ship-ice interaction events

Hans-Martin Heyn[a,*], Roger Skjetne[a]

[a] *Norwegian University of Science and Technology (NTNU), 7491 Trondheim, Norway*

Abstract

During operations with ships in ice-infested waters, vibrations of the hull occur due to ship-ice interaction. The acting ice load and the induced vibrations depend on the ice regime and ice breaking mechanism. Especially crushing of ice against the hull causes high loads against the vessel. The objective of this study is to analyse the frequency components of ice-induced vibrations, measured with accelerometers placed in the bow section of the ship's hull. The Wigner-Ville distribution, which provides a time-frequency representation, is applied on acceleration data collected on the icebreaker Frej during transit in ice-infested Arctic waters. The resulting time-frequency representations show that the excited frequencies depend on the dominant ice breaking mechanism, on the encounter velocity, and on the position of where the ice interaction against the hull occurs. Furthermore, the natural frequencies of the ship's hull change slightly, depending on the conditions on the sea-ice around the vessel. It is concluded that a system of distributed accelerometers on a ship can provide information about the acting ice breaking mechanism, the ice conditions around the vessel, and about the location along the hull, where the ship-ice interaction occurs. This can be used as an additional tool in monitoring systems during operations in ice-infested waters.

Keywords: Arctic, Ship-ice interaction, Acceleration, Wigner-Ville distribution, Time-frequency analysis, Vibrations, Ice load, Marine technology,

*Corresponding author
Email address: martin.heyn@ntnu.no (Hans-Martin Heyn)

1. Introduction

The presence of sea-ice makes operations in the Arctic challenging (Løset et al., 2006). The decay of ice cover in the Arctic region (Lubin & Massom, 2006) will lead to new sea-cargo rutes between Europe and Asia (Arctic Council, 2009). Furthermore, hydrocarbon deposits lie possibly under the seabed of the Arctic oceans (Hossain et al., 2014). Technologies have to be developed to support safe and sustainable operations in the fragile environment of the Arctic. Ice management refers to a system that is capable of reducing the ice loads on a protected vessels to endurable levels (Hamilton et al., 2011). An ice management system can be parted into an ice observer system and a response system (Eik, 2008). The ice observer system requires ice intelligence, which is obtained by collecting and processing information about the ice environment utilising different sensor technologies (Haugen et al., 2011). When a ship operates in ice-infested waters, it is subjected to ice-induced vibrations (Belov & Spiridonov, 2012). The properties of the ice-induced vibration change, depending on the ice interaction mechanism and the ice load affecting the vessel (Yue et al., 2009). In laboratory experiments, Sodhi (1991) showed that the ice-induced vibrations clearly depend on the failure mechanism of the ice. Measuring and evaluating the ice-induced vibrations in real-time could therefore be a reliable source of ice intelligence.

By measuring vibrations on the Finnish icebraker Sisu during ice breaking operations, Matusiak (1982) showed that the additional ice load excites several natural modes of the ship's hull in the bandwidth 2.75 Hz to 7.5 Hz. For a narrow, conical structure, equipped with load panels, Yue et al. (2007) showed that the frequency spectrum of the measured ice loads change under different ice conditions. They used short-time fourier transformation (STFT) for their analysis. The major drawback of the STFT is that the product of time resolution and frequency resolution is constant. It is desired to have a higher frequency resolution at the lower frequency band, in which the ice-induced vibrations typically occur. Bjerkås (2006) overcame this limitation by using a wavelet transformation. Bjerkås et al. (2007) applied a continuous wavelet transformation on ice load signals recorded during ice-structure interaction of a lighthouse in the Gulf of Bothnia. The authors were able to identify intervals of intermittent crushing of ice against the structure, which was the cause of high ice loads and significant vibrations in the structure.

The results from the wavelet transformation can be difficult to interpret, because the resulting spectrum depends on the chosen wavelet function. It is more intuitive to study directly the energy representation of the recorded vibrations and to determine the distribution of the energy content of the vibrations over both frequency and time (Flandrin et al., 2002). The Wigner-Ville distribution is such a joint time-frequency energy density (Boashash, 2003). The vibrations can be recorded with accelerometers placed inside the hull of a ship. Compared to strain gauges or load panels, accelerometers are significantly easier to install and they can be placed anywhere in the ship at little cost and effort.

This study shows that data from accelerometers placed in the hull of a ship, in combination with the Wigner-Ville distribution, provides clear time and frequency information about ice-induced vibrations. The aim is to provide an additional tool for ice condition assessment. Typical ship-ice interaction events as cause for ice-induced vibrations are introduced. A windowed version of the Wigner-Ville distribution, which allows real-time analysis of ice-induced vibrations, is derived. The data from a system of four accelerometers on the icebreaker Frej is used for frequency analysis by the proposed method. In five scenarios, the frequency patterns during ship-ice interaction are analysed and discussed. Because the icebreaker Frej is a sistership of the Finnish icebreaker Sisu, a comparison with the results of Matusiak (1982) is conducted. It is shown that the variations of the natural frequencies of the ship's hull can be tracked in order to assess the ice conditions.

The paper is structured as follows: Section II contains a brief overview of the relevant theory on ship-ice interaction and ice-induced vibrations. Section III

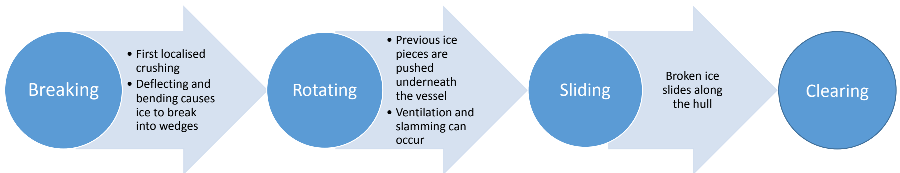

Figure 1: The ice-breaking process under conventional ice conditions.

presents the methodology of the time-frequency decomposition based on the Wigner-Ville distribution. Section IV describes the test setup on the Swedish Atle-class icebreaker Frej and a method to estimate the impact load during the encounter of sea-ice. In Section V the recorded acceleration data and the result from the time-frequency analysis are presented and discussed. Section VI provides a closer analysis of the excitation of natural modes of the ship's hull. Section VII concludes the research results and gives an outlook on future research.

2. Ship-ice interaction

The effects of ship-ice interaction depend on properties of the ship and properties of the ice. When a ship interacts with ice, either by ice drifting towards it or the ship travelling through ice, the ice eventually breaks. The additional loads a ship experiences during the ice-breaking process depend on the failure mode of the ice (ISO/FDIS/19906:2010). During ship-ice interaction, three failure modes play a significant role: Failure due to bending of the ice, failure of the ice by splitting, and failure of the ice by crushing. The active failure mode depends on the shape of the structure (e.g., inclination angle) and several state variables and material properties of the ice (Lu et al., 2015a). State variables are the encounter velocity, the contact area, and the temperature. Some ice properties are the density/porosity of the ice, the ice thickness, and the salinity.

2.1. *Ice loads due to bending failure*

Due to the gravitational force, the structure or vessel pushes the ice downwards. A vertical force component builds up, and once it exceeds the breaking strength of the ice, the ice fails by radial and circumferential cracking. Su et al. (2010) mentions that, due to the periodic characteristic of the process, dominant frequencies in the load by bending failure are identifiable. Yue et al. (2009) identified such regular force patterns for the interaction of ice and a slender vertical monopod structures. Bending failure is the dominant failure mechanism for sloping structures (Løset et al., 2006, Ch. 5), such as in the bow of an icebreaker.

2.2. *Ice loads due to splitting failure*

Besides bending failure, splitting as failure mode can occur especially in level-ice. As in the case of bending failure, a vertical force component builds up and leads to radial and circumferential cracking of the ice. In-plane forces act on the ice floe and on the newly formed crack. Lu et al. (2015b) refers to them as *splitting loads*. They cause an opening of the crack and a propagation of the crack in the ice floe. The propagated crack can extend to a length longer than the structure causing it (Bhat et al., 1991). When the ship propagates into the crack, and thus widens the crack, ice can slide along the hull, which typically cause measurable vibrations.

2.3. *Ice loads due to crushing failure*

Especially at small contact areas, non-sloped contact areas, and high encounter speeds, or with increasing ice thickness, crushing failure becomes the dominant failure mode during ship-ice interaction. The contact area of the ice with the ship or structure is changing randomly, which causes a non-uniform pressure distribution (Løset et al., 2006, Ch. 5) and the production of pulverized material. Due to the random size of the contact area, the load does not show regular frequency patterns. Instead a rather chaotic pattern is observed (Yue et al., 2009), (Masterson et al., 1999).

2.4. The ice-breaking process

According to Riska (2011), Lubbad & Løset (2011), and Su et al. (2010), the ice-breaking occurs generally in four steps, as shown in Figure 1: When the ship encounters an ice floe, the ship's hull and the ice form a small contact area. Due to the small contact area ice crushing will be the dominating failure mode. The ship will proceed further into the ice, which increases the contact area between the hull and the ice. A vertical force component on the ice increases until the bending strength of the ice is reached and ice floes are created by the formation of a bending crack, as described by Riska (2011). The ice pieces start to rotate and to push against the hull. This can cause an additional slamming load against the hull of the vessel (Lubbad & Løset, 2011) and an additional hydrostatic load can occur due to ventilation. This will occur if the gaps between the rotating ice floe and the water surface do not fill up with sea water fast enough. After the rotation process, the ice floe slides along the hull of the vessel until it clears to the sides or gets milled in the propellers of the vessel. If the ice is too strong, for example in the case of multi-year ice, the necessary vertical force component will not exceed the strength of the ice. Instead of bending, the ice will then continue to fail by crushing.

2.5. Ice-induced vibrations

Matusiak (1982) showed that ship vibrations can be regarded as the motions of a forced, damped multi-degree-of-freedom (MDOF) system, given as

$$\mathbf{M}\ddot{\boldsymbol{x}} + \mathbf{C}\dot{\boldsymbol{x}} + \mathbf{G}\boldsymbol{x} = \boldsymbol{\tau}(t), \tag{1}$$

with $\mathbf{M} \in \mathbb{R}^{n\times n}$ is the mass matrix, $\mathbf{C} \in \mathbb{R}^{n\times n}$ is the damping matrix, $\mathbf{G} \in \mathbb{R}^{n\times n}$ is the stiffness matrix, and $\boldsymbol{x} \in \mathbb{R}^{n}$ is the displacement. Upon an external excitation, such as the impact of sea-ice, the hull shows undamped free-vibrations natural modes, denoted ϕ_i, congregated in the modal matrix $\boldsymbol{\Phi} = [\phi_1, \phi_2, \cdots, \phi_n]$. The natural modes of the vessel's hull can be found by solving (2) under a known load:

$$\ddot{\boldsymbol{\eta}}(t) + \mathbf{C}_g\dot{\boldsymbol{\eta}}(t) + \mathrm{diag}(\omega_i^2)\boldsymbol{\eta}(t) = \mathrm{diag}(M_i^{-1})\boldsymbol{f}(t), \tag{2}$$

Table 1: Generalised parameters of the icebreaker Sisu, a sister ship of the icebreaker Frej Matusiak (1982).

Mode	Condition (Ice Thickness)	Natural frequency ω_i	Generalised damping ξ_i	Generalised mass M_i $(kg \cdot m^2)$
1	Open water	2.916 Hz	0.008	0.1180
	30 cm	2.769 Hz	0.053	0.1210
	50 cm	2.703 Hz	0.095	0.1220
2	Open water	5.513 Hz	0.012	0.0201
	30 cm	5.150 Hz	0.054	0.0208
	50 cm	5.078 Hz	0.112	0.0210
3	Open water	7.550 Hz	0.011	0.0047
	30 cm	7.067 Hz	0.046	0.0050
	50 cm	6.594 Hz	0.084	0.0052
4	Open water	9.000 Hz	0.011	0.0036
	30 cm	8.700 Hz	0.044	0.0037
	50 cm	8.312 Hz	0.076	0.0038

where $\mathbf{C}_g = \mathrm{diag}(2\xi_i\omega_i) \in \mathbb{R}^{n\times n}$ is the generalised damping matrix, M_i is the i^{th} generalised modal mass, ξ_i is the damping factor for the i^{th} natural mode, $\boldsymbol{f}(t) = \mathbf{\Phi}^T\boldsymbol{\tau}(t)$ is the generalised force, and $\boldsymbol{\eta} \in \mathbb{R}^n$ is the generalised coordinate vector. Matusiak (1982) showed further that a change in generalised mass can be calculated under the assumption of a velocity and ice thickness independent ship stiffness by

$$M_{i,1} = M_{i,0} \cdot \sqrt{\frac{f_{i,0}}{f_{i,1}}}. \tag{3}$$

The generalised parameters have been identified by Matusiak (1982) for the icebreaker Sisu, a sister ship of the icebreaker Frej. They are summarised in Table 1.

3. Time-frequency analysis of acceleration signals

Changes in the ice failure regime cause changes in the frequency characteristic of the induced vibrations, and ice failure against the hull can also excite the natural modes of the ship's hull. Following the definition of (Boashash, 2003) we require the following results from a time-frequency decomposition:

- Identification of time variations in the signal in order to detect ice interaction events.
- Identification of frequency variations in the signal in order to characterize the ice failure regime and track the excitation of natural frequencies.

3.1. Definition of a signal and its spectrum

The *spectrum* $S(f)$ of a signal $s(t)$ is given by the *Fourier transformation*

$$\begin{aligned} S(f) &= \mathscr{F}\{s(t)\} \\ &= \int_{-\infty}^{\infty} s(t)e^{-j2\pi ft}dt. \end{aligned} \tag{4}$$

A real signal $s(t)$ exhibits *Hermitian symmetry* between the positive-frequency and negative-frequency components of its spectrum (Ohm & Lüke, 2010, Ch. 3).

$$S(-f) = S^*(f) \tag{5}$$

A *stationary signal* $s(t)$ can be written as the sum of cosine-terms and an offset a_0 (Hoffmann & Wolff, 2014, pp. 102-104), as shown in (6).

$$s(t) = a_0 + \sum_{k\in\mathbb{N}} c_k \cos\left(n\omega_0 t + \varphi_k\right) \tag{6}$$

Wave elevations of a long-crested irregular sea, for example, can be described by the sum of harmonic components (Fossen, 2011, Ch. 8.2.3)), implying the assumption of stationarity holds. Ice loads, however, are irregular and highly fluctuating. They are of *non-stationary* character (Bjerkås et al., 2007).

148 *3.2. Energy description of a signal*

The idea of Bjerkås (2006) to use a varying time-frequency decomposition in order to identify different ice load situations will be employed further. But instead of looking at the measured signal directly, an energy definition of the signal will be used. An energy distribution approach is directly applicable to non-stationary and random signals (Matz & Hlawatsch, 2003) and intuitive to interpret. The energy of a signal $s(t)$ in the time-domain is

$$E_s = \int_{-\infty}^{\infty} |s(t)|^2 dt, \tag{7}$$

The energy of a signal in the frequency-domain is equivalently

$$E_s = \int_{-\infty}^{\infty} |S(f)|^2 df, \tag{8}$$

where the term $|S(f)|^2$ is the *energy spectral density.* A joint time-frequency energy density $\rho_s(t, f)$ is then implicitly defined by

$$E_s = \int_{-\infty}^{\infty} \int_{-\infty}^{\infty} \rho_s(t, f) dt df. \tag{9}$$

Such a joint time-frequency energy density must satisfy the *marginal conditions* (Boashash, 2003), which state that if the time-frequency energy density is integrated along one of the variables, the result will be the energy density of the corresponding other variable, that is,

$$\int_{-\infty}^{\infty} \rho_s(t, f) dt = |S(f)|^2 \tag{10}$$

$$\int_{-\infty}^{\infty} \rho_s(t, f) df = |s(t)|^2. \tag{11}$$

149 *3.3. Wigner distribution*

A joint time-frequency energy density, that fulfils the marginal conditions (10) and (11), is the Wigner distribution. The kernel $K_s(t, \tau)$ of the distribution is based on the autocorrelation function of the signal, given by

$$K_s(t, \tau) = s\left(t + \tfrac{\tau}{2}\right) s^*\left(t - \tfrac{\tau}{2}\right). \tag{12}$$

The Fourier transformation of the kernel leads further to a time-frequency energy density, denoted $W_s(t,f)$, defined as

$$\begin{aligned}\rho_s(t,f) &= \mathscr{F}\{K_s(t,\tau)\} \\ &= \int_{-\infty}^{\infty} s\left(t+\tfrac{\tau}{2}\right) s^*\left(t-\tfrac{\tau}{2}\right) e^{-j2\pi f\tau} d\tau \qquad (13) \\ &= : W_s(t,f). \qquad (14)\end{aligned}$$

As a quadratic time-frequency distribution, the Wigner distribution leads to artefacts that compromise the interpretability of the time-frequency distribution image. An example of this effect is given in the Appendix.

3.4. Wigner-Ville distribution

The Wigner-Ville distribution can be defined exactly as the Wigner distribution (13) except for the chosen signal. Instead of the signal $s(t)$, the analytic associate $s_+(t)$ is used, which eliminates the frequency interference terms from the distribution. The analytic associate is defined by

$$s_+(t) = s(t) + j\mathscr{H}\{s(t)\}, \qquad (15)$$

where $\mathscr{H}\{s(t)\}$ describes the *Hilbert transformation*, which removes the negative frequency components from the original signal $s(t)$. Due to the Hermitian symmetry (5), no information is lost. The Wigner-Ville distribution is then defined as

$$\begin{aligned}W_{s_+}(t,f) &= \mathscr{F}\{K_{s_+}(t,\tau)\} \\ &= \int_{-\infty}^{\infty} s_+\left(t+\tfrac{\tau}{2}\right) s_+^*\left(t-\tfrac{\tau}{2}\right) e^{-j2\pi f\tau} d\tau. \qquad (16)\end{aligned}$$

The kernel $K_{s_+}(t,\tau)$ is referred to as *instantaneous autocorrelation function* (Boashash, 2003).

3.5. Windowed Wigner-Ville distribution

The signal $s_p(t)$ is time-limited and obtained by multiplying the signal $s(t)$ with a window function $h(t)$. The Wigner-Ville distribution is applied on the corresponding analytic associates of the signals,

$$
\begin{aligned}
&W_{s_{p,+}}(t,f) \\
&= \int_{-\infty}^{\infty} h(\tau) s_+\left(t+\tfrac{\tau}{2}\right) s_+^*\left(t-\tfrac{\tau}{2}\right) e^{-j2\pi f\tau} d\tau.
\end{aligned}
\tag{17}
$$

The window function $h(t)$ causes a frequency smoothing of the time-frequency distribution (Boashash, 2003, Ch. 2.1.4.3). The use of a window function will be necessary when the system is used in a real-time system, where a sliding window function selects the available data for analysis.

3.6. Aspect of the application of the Wigner-Ville distribution on ice-induced acceleration signals

The Wigner-Ville distribution has several positive properties that are beneficial for the analysis of ice induced acceleration signals. Some important properties are summarised here, as from Flandrin (1999) and Boashash (2003).

- *Time-shift invariance*: A time shift in the signal s_+ causes the same time shift in $W_{s_+}(t,f)$. This allows moving time windows for analysing the ice induced signals in a real-time system.

- *Frequency-shift invariance*: A frequency shift in the signal s_+ causes the same shift in frequency in $W_{s_+}(t,f)$. This is needed to identify varying frequency components in the time-frequency distribution of the acceleration signals.

- *Instantaneous frequency*: The mean of the Wigner-Ville distribution is the instantaneous frequency of the signal.

- *Marginal conditions*: The Wigner-Ville distribution fulfils the marginal conditions (10) and (11). That allows the calculation of the instantaneous power (7) and the energy spectrum of the signal (8) from the distribution.

- *Global energy*: The total energy of the signal can be evaluated with (9). This ensures that energy-changes caused by the ice interaction can be identified from the distribution.

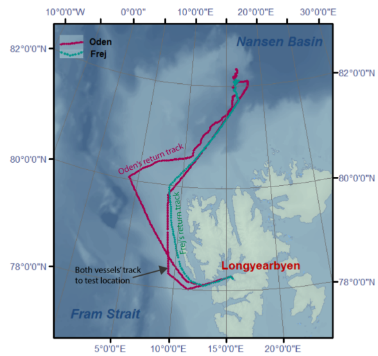

Figure 2: Track of the icebreakers Frej and Oden (Courtesy of Wenjun Lu).

- *Compatibility with filtering*: A convolution of two signals results in a convolution of the Wigner-Ville distributions of these two signals. This property ensures that an ice load signal can be filtered, e.g. by a lowpass filter.

- *Non-stationary signals*: It is shown by Matz & Hlawatsch (2003) that the Wigner-Ville distribution can generally also be applied on non-stationary random signals $s_r(t)$. Instead of the total energy of the signal, the mean energy is obtained by

$$\int_{-\infty}^{\infty}\int_{-\infty}^{\infty} W_{s_{r,+}} dtdf = E\{||s_r||^2\}. \tag{18}$$

4. A measurement system for ice induced accelerations

This section describes the measurement setup for collecting ice-induced acceleration data during an Arctic expedition with the Swedish icebreaker Frej in the Arctic Ocean north of Svalbard in September 2015.

4.1. The Oden Arctic Technology Research Cruise 2015

The Oden Arctic technology research cruise took place in September 2015 in the Arctic Ocean north of Svalbard with the two icebreakers Oden and Frej. The track of the expedition is shown in Figure 2, and general information about the expedition can be found in Lubbad et al. (2016).

Table 2: Technical specifications of icebreaker Frej (Lubbad et al., 2016)

Icebreaker Frej	
Length	107.75 m
Beam	31.20 m
Draft	7.0 m - 8.5 m
Power generation	18.6 MW
Speed in open waters	18 kts
Icebreaking capability	1.2 m at 3 kts
Displacement	7800 t
Hydro. damping d_{11}	$2.14 \cdot 10^4\ kg \cdot s^{-1}$

Frej is an Atle-class icebreaker, commissioned in 1975. The propulsion system consists of two fore and two aft propellers and a diesel-electric power-plant with four diesel generators. Up to three auxiliary generators provide electricity for the ship. In normal operations the generators for the propulsion system run at 495 rpm and the auxiliary generators run at 750 rpm. This information is important since the generators induced a constant vibration into the ship, which is noticeable in the vibration measurements. Table 2 summarises the technical specifications of the icebreaker.

4.2. Sensor configuration and specification

Four inertial measurement units (IMU) from Analog Devices were installed at various positions of the vessel; see Figure 3. An IMU contains a tri-axis angular rate sensor and a tri-axis acceleration sensor, as illustrated in Figure 4. Only the accelerometer data were used in this study.

One sensor (*ADIS 16480*) was placed on Deck 9, underneath the bridge level, on a firm metal beam to serve as a reference sensor. Three sensors (*ADIS 16364*) were placed in a storage compartment in the bow, close to the ice interaction zone of the vessel. The sensors in the bow compartment were placed port, mid-ship, and starboard. The port- and starboard sensors were placed on

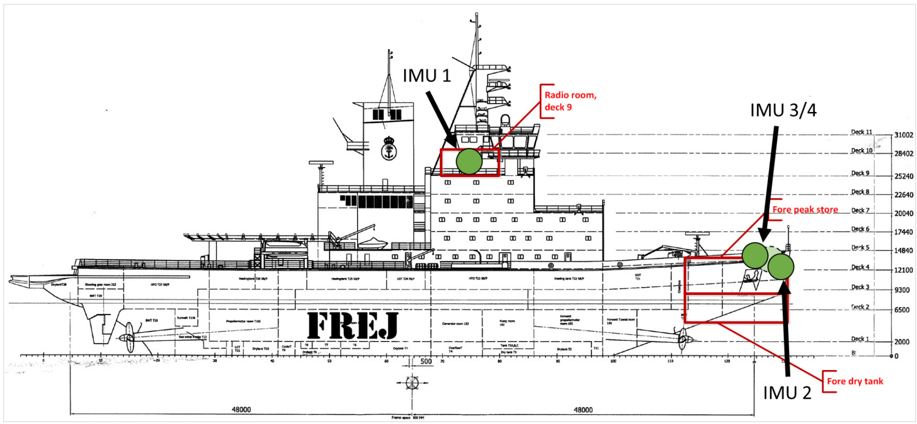

Figure 3: Position of the motion sensors.

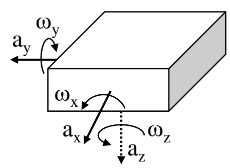

Figure 4: IMU sensor with three accelerometers and three gyros

beams directly connected to the hull of the ship. The compartment was heated to a constant temperature of 18°C, which minimised temperature related biases on the measurements. The *ADIS 16480* sensor contained additionally a tri-axis magnetometer, which was not used in this study.

A central server collected the data from the individual IMUs and served as time synchronisation server for the sensor units. To ensure time synchronisation during the measurements, a real-time clock in each of the sensor units was continuously synchronised with the GPS-time obtained from the ship systems. Furthermore, synchronised data from other ship systems such as the GPS system, the gyrocompass, and wind sensors, were collected. Images from a 360° camera system and two 180° cameras were also collected, synchronised and processed in order to identify the ice conditions around the vessel.

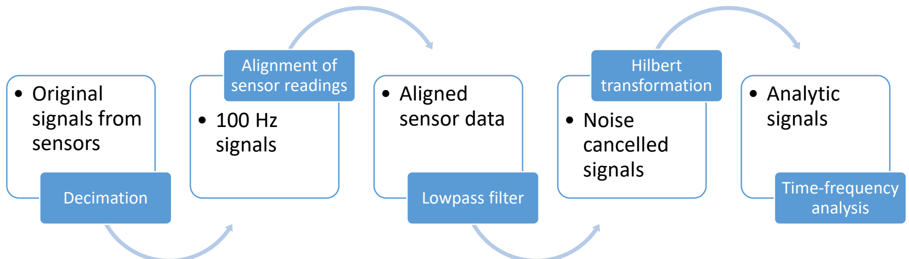

Figure 5: Pre-processing steps for the signals from the accelerometers

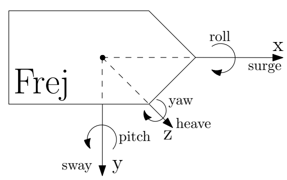

Figure 6: Body-fixed coordinate system definition.

4.3. Preprocessing of sensor readings

To minimise the influence of sensor noise, to align the sensor readings and to remove the influence of cross terms in the time-frequency distribution, several preprocessing steps were executed, as summarised in Figure 5.

4.3.1. Decimation of sensor signals

The sensors were operated with a sampling rate of 300 Hz. For the ice-induced vibrations, such a high sampling rate is not required since the ship's structure damps high frequency vibrations. To achieve a faster processing speed of the data, the signals were decimated to 100 Hz.

4.3.2. Alignment of sensor readings

For the alignment of the sensors, a body-fixed ship-wide coordinate system according to Fossen (2011) is defined, as shown in Figure 6.

At the location of the sensor, the sensor's coordinate system is not aligned with the body-fixed coordinate system. The accelerations measured by any of the sensors in its coordinate system are denoted $\boldsymbol{a}_i^s$, and referred to as proper

Table 3: Sensor orientation in relation to the body-fixed coordinate system of the ship

	IMU 1	IMU 2	IMU 3	IMU 4
ϕ	$180.18°$	$-1.06°$	$2.10°$	$-0.83°$
θ	$-0.12°$	$208.73°$	$204.86°$	$203.94°$
ψ	$0°$	$0°$	$-90.00°$	$90.00°$

acceleration. The corresponding acceleration vector in the body-fixed coordinate system is denoted $\boldsymbol{a}_i^b$. The orientation-matrix $\boldsymbol{\Theta}_{\boldsymbol{s},\boldsymbol{i}} = [\phi_i, \theta_i, \psi_i]^T$ states the orientation of each sensor's coordinate system relative to the body-fixed coordinate system. The orientation matrices for the four sensors are given in Table 3. A rotation matrix $\mathbf{R}_{s_i}^b(\boldsymbol{\Theta}_{s,i})$, as the result of a rotation sequence, is applied to transform all sensor readings into the body-fixed coordinate system of the ship (Fossen, 2011), according to

$$\boldsymbol{a}_i^b = \mathbf{R}_{s_i}^b(\boldsymbol{\Theta}_{s,i})\boldsymbol{a}_i^s, \tag{19}$$

with

$$\mathbf{R}_{s_i}^b(\boldsymbol{\Theta}_{\boldsymbol{s},\boldsymbol{i}}) = \mathbf{R}_{z,\psi_i}\mathbf{R}_{y,\theta_i}\mathbf{R}_{x,\phi_i}.$$

4.3.3. Lowpass and Hilbert filter

The signal has to be converted into an associated analytic signal in order to minimise the influence of cross terms in the time-frequency distribution. A lowpass filter removes high frequency noise components above 45 Hz from the signal. The sensors were calibrated and operated under a constant temperature in order to avoid a temperature related bias in the measurements.

4.4. Impact load estimation from acceleration measurements

Under the assumption that sensor noise, biases, and the earth gravity influence are removed from the measurements, and that the influence of wind and waves can be neglected, the measured acceleration in the body-fixed coordinate system is

$$\boldsymbol{a}_i^b = \boldsymbol{a}_{hyd}^b + \boldsymbol{a}_{prop}^b + \boldsymbol{a}_{ice}^b + \boldsymbol{a}_{vib,i}^b, \tag{20}$$

with $\boldsymbol{a}^b_{hyd} \in \mathbb{R}^3$ describing the global hydrodynamic load, $\boldsymbol{a}^b_{prop} \in \mathbb{R}^3$ the global propellers' induced load, $\boldsymbol{a}^b_{ice} \in \mathbb{R}^3$ the global ice induced load, and $\boldsymbol{a}^b_{vib,i} \in \mathbb{R}^3$ the locally induced vibrations.

With a constant speed and heading just before the impact with an ice feature, it can be assumed that the propeller thrust compensates for the hydrodynamic forces acting against the travel direction of the vessel. If the acceleration is measured at a location with sufficient damping from locally induced vibrations, such that these can be neglected, the measured acceleration in surge direction will consist of the global ice induced impact load:

$$a^b_{ice,surge} = \mathbf{B}_x \mathbf{R}^b_{s_i}(\psi_i)\boldsymbol{a}^s_i, \tag{21}$$

where $\mathbf{B}_x = (1, 0, 0)$ selects only the surge acceleration. With information about the ship's mass m_{ship}, added mass m_{add} (assumed as 20% of m_{ship} for this study), linear hydrodynamic damping d_{11} for the surge direction, and velocity u_{surge}, the force acting against the vessel in surge direction is

$$F_{surge} = m_{11}(a^b_{ice,surge} + d^{-1}_{11} u_{surge}), \tag{22}$$

with

$$m_{11} = m_{ship} + m_{add}. \tag{23}$$

5. Time-frequency distributions of ship-ice interaction events

In this section several cases of ship-ice interaction events of the icebreaker Frej in the Arctic Ocean are analysed in regards to the excited frequencies in the hull vibration with the help of the Wigner-Ville distribution. The data for the cases 1 to 4 have been collected on the 26th September 2015 between 11:00 UTC and 12:00 UTC. The track of the ship is illustrated in Figure 21. The relative wind speed was measured to be between 1 m/s and 6 m/s in the mentioned period. The influence of wind loads on the ice are neglected due to the low wind speeds. An overview of the analysed data is given in Table 4.

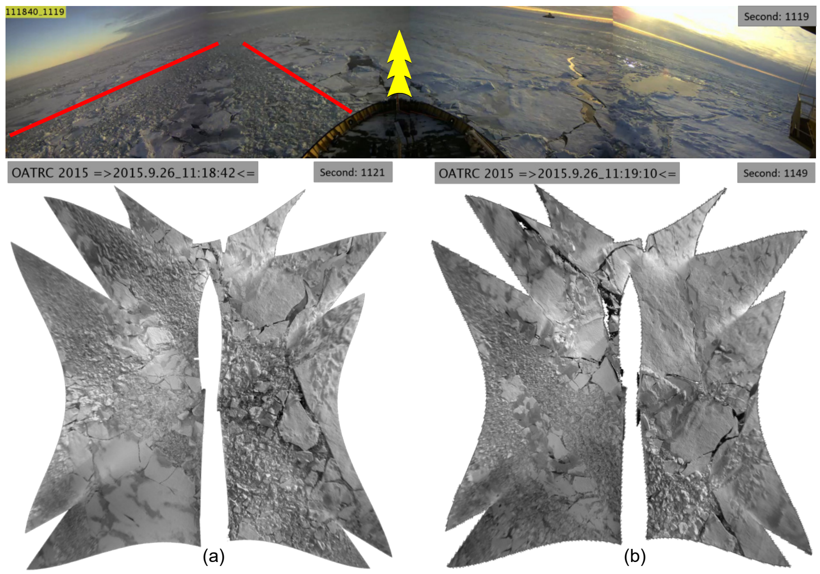

Figure 7: Case 1: Ship leaving a channel of broken ice (a) and transits into unbroken ice (b).

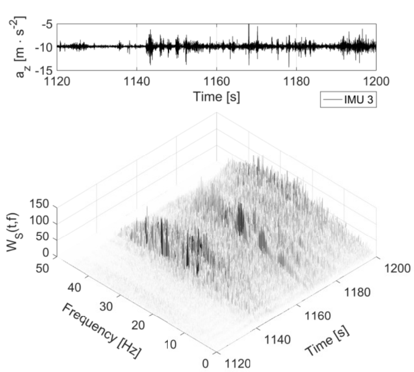

(a) Port sensor

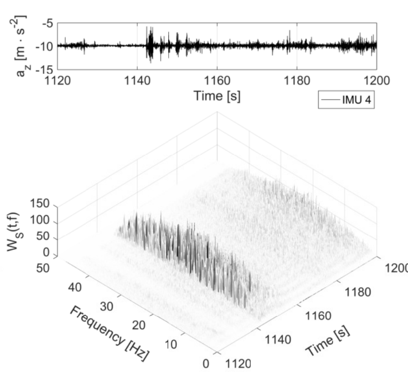

(b) Starboard sensor

Figure 8: Case 1: Time-frequency distributions of the vertical acceleration.

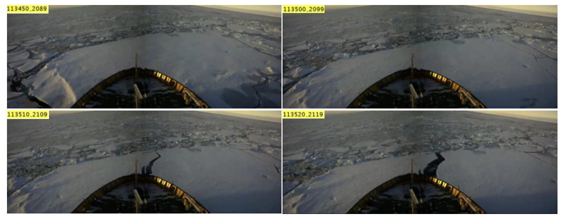

Figure 9: Case 2: Ship encounters an unbroken ice floe which splits upon impact.

Figure 10: Case 2: Crushing ice at starboard bow hull section just before splitting occurs.

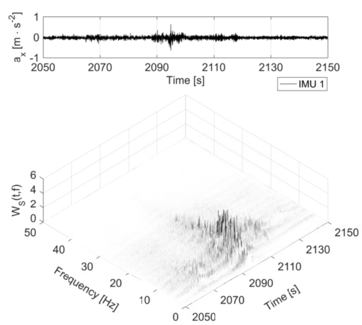

(a) Deck 9 sensor

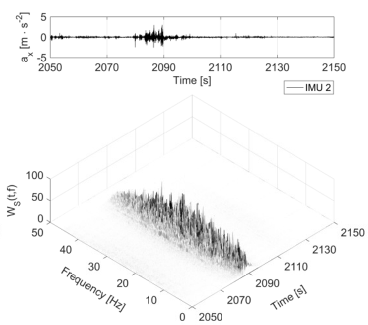

(b) Midship sensor

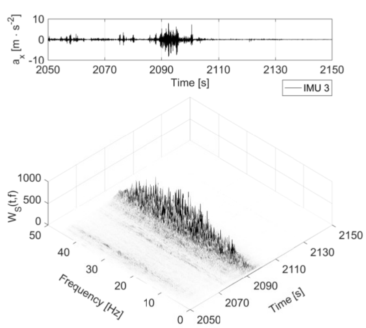

(c) Port sensor

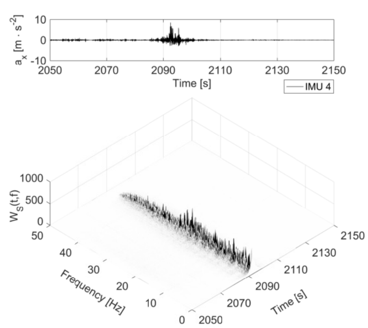

(d) Starboard sensor

Figure 11: Case 2: Time-frequency distributions of the x-acceleration.

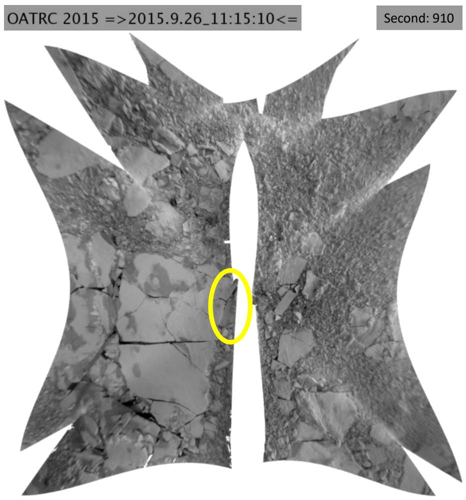

Figure 12: Case 3: One piece of ice gets flipped by the ship.

Figure 13: Case 3: Broken ice floe at the port side of the vessel.

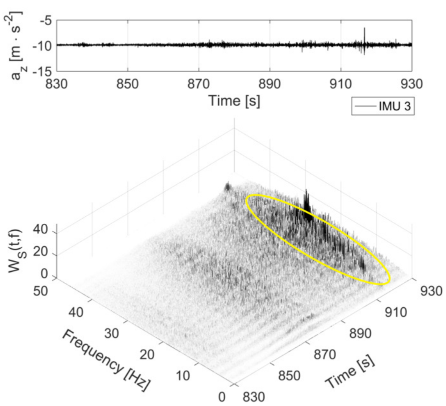

(a) Port sensor

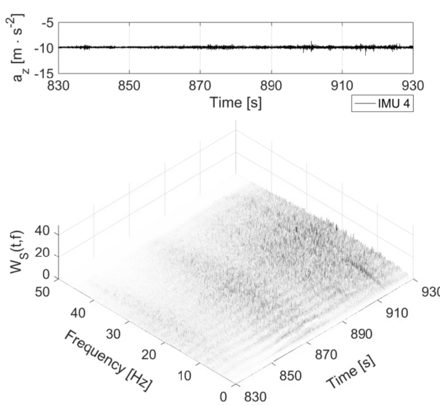

(b) Starboard sensor

Figure 14: Case 3: Time-frequency distributions of the vertical acceleration.

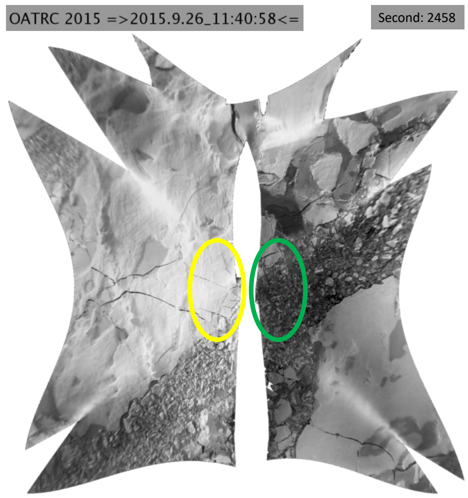

Figure 15: Case 4: Ice fails at port side of the ship (marked yellow) while starboard side encounters broken ice pieces (marked green).

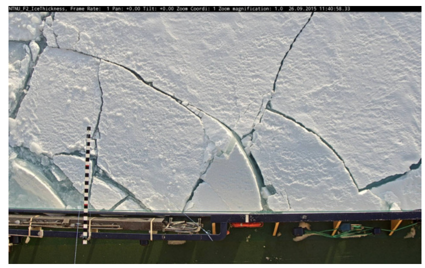

Figure 16: Case 4: Close-up view of yellow marked area in Figure 15. The measuring beam raster is 10 cm per block and has been mounted about 3 m above the ice. The camera is installed 20 m above the ice. Therefore the lengths taken from the measuring beam has to be multiplied by a factor of 1.2.

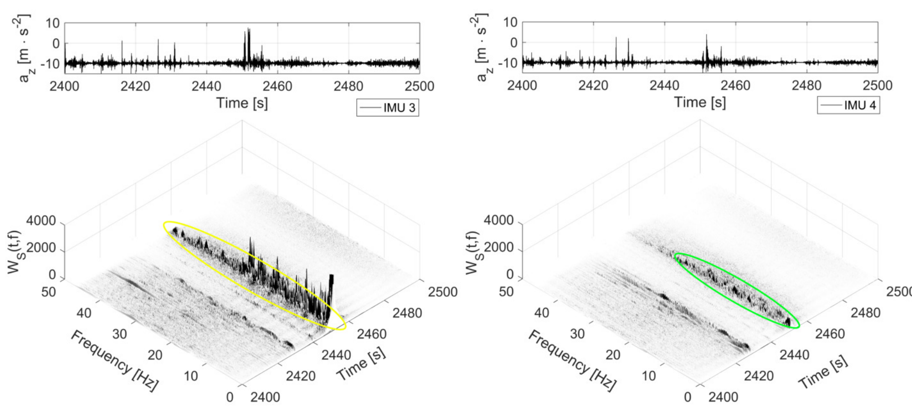

(a) Port sensor

(b) Starboard sensor

Figure 17: Case 4: Time-frequency distributions of the z-acceleration during one-sided encounter of a large piece of ice in a broken ice field.

Table 4: Overview of analysed measurements

Case	Date	Seconds in measurement	Ice conditions	Ice thickness	Speed over ground
1	26.09.2017 11:19.40	1120 - 1200	Transit from broken ice to unbroken very close pack-ice	0.5 m - 1.0 m	3.58 knots
2	26.09.2017 11:34.10	2050 - 2150	Broken ice, encounter of unbroken ice floe of ∼100 m diameter	0.7 m	2.97 knots
3	26.09.2017 11:13.50	830 - 930	Broken ice, flipping of ice pieces on port side	0.3 m - 0.5 m	3.74 knots
4	26.09.2017 11:40.00	2400 - 2500	Broken ice on starboard close pack-ice on port	0.5 m - 0.7 m	4.33 knots
5	30.09.2017 10:47.40		Open-water		10.50 knots

5.1. Case 1: Transition from managed ice to unmanaged ice

The icebreaker Frej travelled at a speed of 3-4 knots inside an ice-channel created by the second icebreaker Oden. At second 1140, Frej moved out of the ice channel and hit a field of unbroken ice with an angle of about 45°. The ice was first-year ice with a thickness of 0.5 m to 1 m. The situation is shown in Figure 7.

Figures 8a) and 8b) show the time-frequency distribution of the ship's vertical acceleration measured by the sensors IMU 3 and IMU 4, which were placed in the bow section of the vessel. While moving in managed ice (seconds 1100-1140), significant vibrations in the hull are not noticeable. Upon entering the unbroken ice field at second 1141, the ice around the vessel failed by crushing and bending of the ice. The transition into unbroken ice is clearly visible in the time-frequency distribution due to a significant increase of energy of the signal over all frequencies. Especially vibrations with frequencies between 15 Hz and 30 Hz have a higher energy. After a few seconds the excitation decreases, but the energy of the vibrations is still significantly higher than when travelling in the broken ice.

The significant excitations upon exiting the ice channel can be connected to a sudden decrease in velocity of the vessel, which was observed. The kinetic energy upon contact with the unbroken ice might have caused a significant amount of crushing prior to bending of the ice. As soon as the ship's speed decreased, bending failure might have become the dominating failure mode again. This created significantly less vibrations than crushing, but still more than in the case of ice-interaction with already broken ice inside the ice channel.

5.2. Case 2: Splitting of a major first-year ice floe

The ship encountered an unbroken ice floe with a characteristic length of about one ship length while travelling at about 3 knots through a field of broken ice. Upon impact the ship got significantly decelerated, nearly to a standstill. After about 15 seconds the ice floe split, and the ship moved ahead into the opening crack. The situation is shown in Figure 9.

The resulting time-frequency distributions for the x-acceleration signals of all four sensors are shown in Figure 11. The energy of the vibrations measured by the two sensors placed directly on the hull of the vessel (sensors IMU 3 and IMU 4) is significantly stronger between 2085 and 2010 seconds. The midship sensor IMU 2 captured the vibration over all frequencies but with a tenth of the energy content as the sensors placed directly on hull. The reason is that the sensor IMU 2 was not placed directly on a hull segment but on a bearing beam of the foredeck. The sensor on Deck 9 (IMU 1) could not measure signal components over 20 Hz, which is due to damping of the superstructure.

It is notable, that major vibrations occur prior to the actual splitting of the ice floe. The reason might be that, due to the propagating ship, crushing occurred while the overall stress on the ice floe had increased. Upon splitting, the measured vibrations decay as the ship moves forwards inside the crack. Instead of failing, the ice was pushed away from the ship. In Figure 10 the starboard hull section of the bow of the vessel is shown just before the splitting has occurred. Crushing of ice is visible along the hull of the vessel (see yellow marked area in the image) and it might be the cause for the broadband vibrations in the time-frequency distribution.

5.3. Case 3: Port side contact with larger ice piece in broken ice field

While travelling in a field of broken ice, the ship encountered several pieces of a broken ice floe on the port side. The situation is shown in Figure 12. While moving forward, the port section of the hull of the vessel got in contact with one piece of the broken ice floe and flipped it, as shown in the yellow marked area in Figure 13. The first-year ice had a thickness of estimated 30 to 50 cm and the ship travelled at about 3-4 knots.

Figure 14 shows the time-frequency distributions for the vertical accelerations measured by the hull mounted sensors. The energy content of the signals is low, because the ship moved in already managed ice. During the time of hull contact with a piece of the broken ice floe, the port mounted sensor (IMU 3) recorded an increase in vibration energy, especially in the frequencies 5 Hz - 15 Hz. The starboard sensor (IMU 4) did not record any significant change in the energy of the vibrations.

Since the piece of ice got only in contact with the port section of the hull, it makes sense, that the sensor on this side recorded the vibrations, which could have been caused by sliding of the ice piece along the hull while it flipped. The energy content of the measured vibrations is much lower than in the previous Case 2, where crushing against the hull occurred. The kinetic energy of the impact went into the rotational movement of the ice piece, and no failure of the ice piece occurred.

5.4. Case 4: Bending failure on one shipside

The ship hit unbroken level-ice on the port side while travelling in a channel of broken ice. The first-year level-ice had a thickness of 50 to 70 cm. While propagating forward the unbroken ice at the port side of the ship failed by forming circumferential and radial cracks, as shown in Figure 15 and, in more detail, in Figure 16. The sea-ice consisted of small broken ice pieces at the

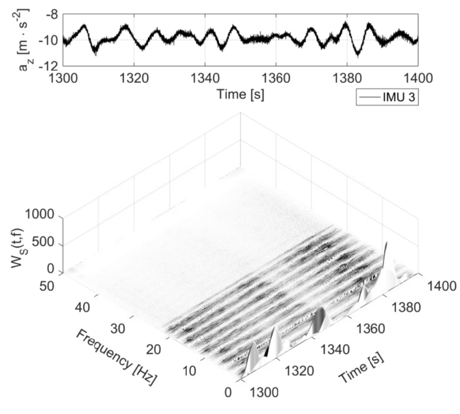

Figure 18: Case 5: Time-frequency distributions of the vertical acceleration (IMU 3)

starboard side of the ship.

The time-frequency distribution for the vertical accelerations measured by the hull mounted sensors IMU 3 and IMU 4 are shown in Figure 17. The bending failure occurred between seconds 2450 and 2460. Both sensor registered the ice interaction. However, the energy of the measured vibrations on the side of impact, the port side, is significantly higher. Most energy is contained in the range of frequencies between 5 Hz and 25 Hz.

The high energy content of the measured accelerations must be a result of the circumferential and radial cracking, as shown in Figure 16. In contrast to Case 3, where the piece of ice just flipped around without breaking, the ice floe actually failed against the hull of the vessel, which induced significant broadband vibrations.

5.5. Case 5: Measurements in open water during a severe sea state

The ship encountered a storm on the return journey to Svalbard while travelling in open water without any ice interaction. The significant wave height was estimated to be between 5 and 7 metres. The data was recorded on the 30th September 2015. The resulting time-frequency distribution for the measured vertical acceleration of IMU 3 is shown in Figure 18. The most obvious property of the time-frequency distribution of the recorded vertical acceleration is the high energy content at the typical wave frequencies below 1 Hz. Furthermore, the ship hull's natural frequencies are visible. In contrast to ice-induced vibrations, there are no broadband impact events.

6. Excitation of natural frequencies of the hull

6.1. Tracking of the first natural frequency during transit in ice

In all cases, the natural modes of the hull were excited and the natural frequencies can be seen in the time-frequency distributions. A closer look at the spectral densities for different scenarios is given in Figures 19 and 20. Significant energy is contained in vibrations at around 2.72 Hz-2.75 Hz, 5.02 Hz-5.08 Hz, and 8.05 Hz and 9.85 Hz. The two frequencies around 2.72 Hz and 5.02 Hz correspond to the natural frequencies found by Matusiak (1982), see Table 1. The vibrations with 8.05 Hz must be originated in the engines, since the main engines ran normally at 495 rpm, which equals a frequency of about 8.25 Hz. The frequency at 9.85 Hz can be another higher natural mode, not present during the measurements on the sistership Sisu in 1982. It has to be noted, that the ship Frej has been significantly modified since it's launch in 1975.

Matusiak (1982) mentions that the first natural frequency decreases, depending on the ice thickness, when travelling in ice. To investigate this behaviour, the resulting Wigner-Ville distribution was used to automatically determine the first natural frequency in the measured acceleration signal of IMU 1 during transit in an ice field with broken and unbroken ice, as illustrated in Figure 21. The result of the tracking of the first natural frequency is presented in Figure 22, and plotted together with the estimated ice induced impact load. The impact load has been calculated from the measurements of IMU 1 using (22), and the parameters given in Table 2. A lowpass filter, set with a cut-off frequency at 7.5 Hz was applied to the acceleration signal. A running average filter has been applied on the resulting load estimate in order to make the load trend better.

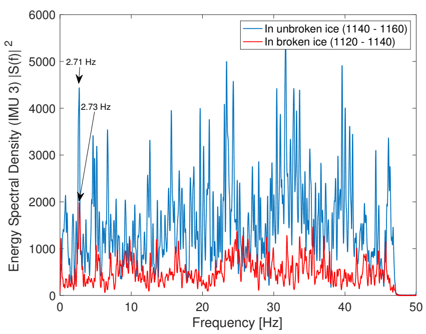

(a) Port sensor

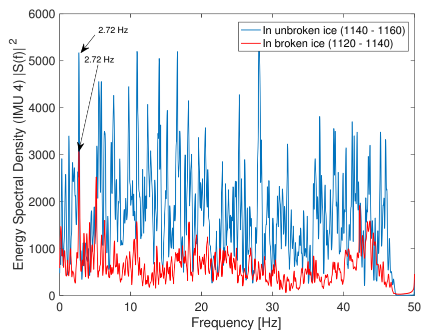

(b) Starboard sensor

Figure 19: Case 1: Energy spectral density of the vertical acceleration during transit from broken to unbroken ice.

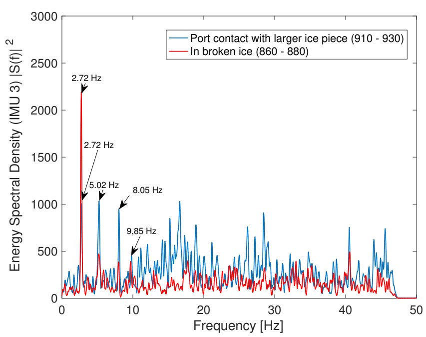

(a) Port sensor

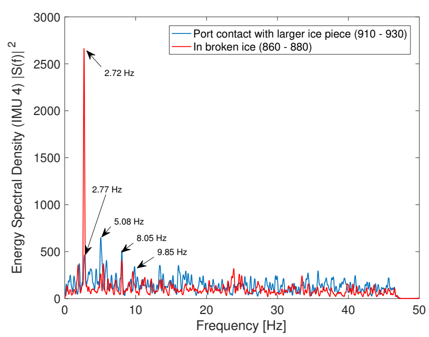

(b) Starboard sensor

Figure 20: Case 3: Energy spectral density of the vertical acceleration during port-sided encounter of a larger piece of ice.

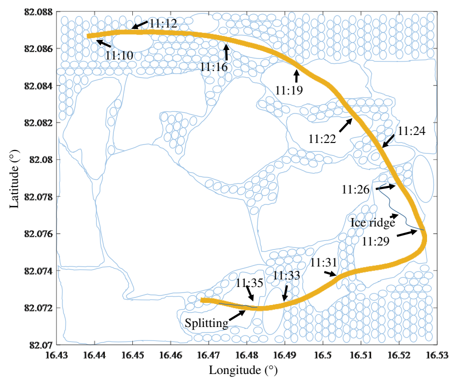

Figure 21: Illustration of encountered icefield

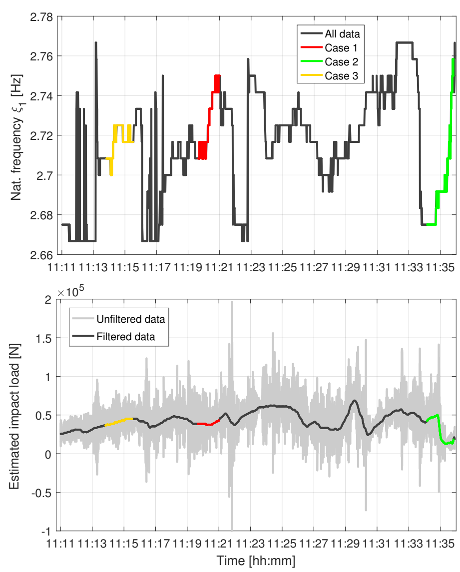

Figure 22: Track of first natural frequency and estimated impact load during transit in icefield

The first natural frequency ξ_1 measured by IMU 1 occurs in the frequency band 2.67 Hz to 2.77 Hz. It is notable, that a lower first natural frequency (lower than 2.70 Hz) occurs always during an increase in induced ice load and upon impact with an unbroken ice floe. A higher first natural frequency (higher than 2.74 Hz) corresponds with transit in broken ice between the unbroken ice floes.

7. Conclusion

This study proposed the Wigner-Ville distribution for the time-frequency analysis of ice-induced accelerations during transit with an Atle-class icebreaker. The resulting time-frequency spectra motivates the development of accelerometer based sensor system for ships operating in ice-infested waters.

The interaction with sea-ice induces vibrations into the ship's hull with frequency components up to 25 Hz, and especially crushing as failure mode induces high-frequency vibration in the hull of the vessel. Natural frequencies of the ship's hull up to 7.5 Hz are globally measurable, and high-frequency vibration are only locally measurable. Measuring ice induced accelerations locally at several points along the ship's hull allows therefore for the localisation of ice action against the ship along the ship's hull. Each failure regimes of the ice induces a unique frequency pattern, which allows for the detection of the acting failure mode during ship-ice interaction.

Accelerometers are capable of tracking the excitation of the ship's hull natural frequencies. Depending on the ice-condition around the vessel, the natural frequencies change. Matusiak (1982) claimed that this change in the natural frequencies is due to a change in added mass when an ice floe is attached to the ship's hull. It was shown, that a lower first natural frequency occurs upon impact of the vessel with an unbroken ice floe (Case 3). Just before the splitting occurred, the ship's bow was well pressing against the unbroken ice floe and the measured first natural frequency decreased to 2.675 Hz. After splitting had occurred, the bow of the vessel moved into the open water inside the split and the first natural frequency increased to 2.760 Hz, which, according to (3) corresponds to a loss of mass of 1.55%. The reason can be, that the additional mass of the ice floe was not in contact with the ship's hull anymore.

7.1. Further work

The shift of natural frequency upon impact with ice floe can be used for an estimation of the ice mass during ship-ice interaction, as already mentioned by Matusiak (1982). With the addition of IMUs on a vessel, a system could be realised, that estimates in real-time the mass of any ice feature the ship get in contact with. By locally tracking high frequent vibrations in the hull, a warning upon occurrence of crushing against the hull can be issued to the crew of an ice-going vessel.

Only global and local acceleration measurements during transit were available for this study. Additional work should be conducted in collecting acceleration data during stationkeeping, and analyse if scenarios like accumulation of ice on one side of the stationkeeping vessel can be detected with local vibration measurements in the hull.

Acknowledgement

The authors would like to thank the Research Council of Norway (RCN) for financial support through projects 203471 CRI SAMCoT and 223254 CoE AMOS. Oden Arctic Technology Research Cruise 2015 (OATRC2015) was supported by the ExxonMobil Upstream Research Company and performed by the Norwegian University of Science and Technology (NTNU) through the SAMCoT CRI and in cooperation with the Swedish Polar Research Secretariat (SPRS) and the Swedish Maritime Administration (SMA). Furthermore, the authors are grateful for the extraordinary hospitality and support received from the crews of the icebreakers Frej and Oden and the Swedish Maritime Administration (SMA).

The authors would like to thank Professor Sveinung Løset, Professor Raed Lubbard, Dr. Wenjun Lu, Dr. Øivind Kjerstad, and Thorvald Grimstad for their help, input, and valuable discussions during and after the expedition.

Appendix

Interference term in the Wigner distribution. An example from (Boashash, 2003) explains the interference effect: A signal with constant frequency f_c is given as

$$s(t) = \cos(2\pi f_c t).$$

The kernel of the corresponding Wigner distribution is given by:

$$\begin{aligned} K_s(t,\tau) &= s\left(t+\tfrac{\tau}{2}\right) s^*\left(t-\tfrac{\tau}{2}\right) \\ &= \cos\left(2\pi f_c \left(t+\tfrac{\tau}{2}\right)\right)\cdot\cos\left(2\pi f_c\left(t-\tfrac{\tau}{2}\right)\right) \\ &= 0.5\cdot\cos\left(2\pi f_c \tau\right) + 0.5\cdot\cos\left(2\pi f_c t\right), \end{aligned}$$

and the Fourier transformation leads further to the time-frequency energy density

$$\begin{aligned} W_s(t,f) &= \mathscr{F}\{K_s(t,\tau)\} \\ &= 0.25\cdot\delta(f-f_c) + 0.25\cdot\delta(f+f_c) \\ &\quad +0.5\cdot\cos\left(4\pi f_c t\right)\delta(f). \end{aligned} \tag{24}$$

The last term in (24) is the interference between the positive- and negative frequency components of the real signal (Boashash, 2003).

References

Arctic Council (2009). *Arctic Marine Shipping Assessment 2009 Report*. Technical Report Arctic Council.

Belov, I. M., & Spiridonov, N. N. (2012). Features of Ship Vibration in Ice Operation Conditions. *Twenty-second (2012) International Offshore and Polar Engineering Conference*, *4*, 1223–1228.

Bhat, S. U., Choi, S. K., Wierzbicki, T., & Karr, D. G. (1991). Failure analysis of impacting ice floes. *Journal of Offshore Mechanics and Arctic Engineering*, *113*, 171–178.

Bjerkås, M. (2006). Wavelet transforms and ice actions on structures. *Cold Regions Science and Technology*, *44*, 159 – 169.

Bjerkås, M., Skiple, A., & Iver Røe, O. (2007). Applications of continuous wavelet transforms on ice load signals. *Engineering Structures*, *29*, 1450–1456.

Boashash, B. (2003). *Time Frequency Signal Analysis and Processing*. Elsevier.

Eik, K. (2008). Review of experiences within ice and iceberg management. *The Journal of Navigation*, *61*, 557–572.

Flandrin, P. (1999). *Time-frequency/time-scale analysis* volume 10. London: Academic Press.

Flandrin, P., Auger, F., & Chassande-Mottin, E. (2002). Time-frequency reassignment from principles to algorithms. chapter Chapter 5. (pp. 179–203). CRC Press.

Fossen, T. I. (2011). *Handbook of marine craft hydrodynamics and motion control*. Wiley & Sons, Ltd.

Hamilton, J., Holub, C., Blunt, J., Mitchell, D., & Kokkinis, T. (2011). Ice management for support of arctic floating operations. In *Arctic Technology Conference*.

Haugen, J., Imsland, L., Løset, S., , & Skjetne, R. (2011). Ice observer system for ice management operations. In *Proceedings of the Twenty-first International Offshore and Polar Engineering Conference*.

Hoffmann, R., & Wolff, M. (2014). *Intelligente Signalverarbeitung 1*. Springer Vieweg.

Hossain, K., Koivurova, T., & Zojer, G. (2014). Arctic marine and governance and opportunities for and transatlantic cooperation. chapter Understanding Risks Associated with Offshore Hydrocarbon Development. (pp. 159 – 176). Springer.

ISO/FDIS/19906:2010 (2010). Petroleum and natural gas industries - Arctic offshore structures. International Organization for Standardization, Geneva, Switzerland.

Løset, S., Shkhinek, K. N., Gudmestad, O. T., & Høyland, K. V. (2006). *Actions from Ice on Arctic Offshore and Coastal Structures*. LAN.

Lu, W., Lubbad, R., Høyland, K., & Løset, S. (2015a). Physical model and theoretical model study of level ice and wide sloping structure interactions. *Cold Regions Science and Technology*, *101*, 40–72.

Lu, W., Lubbad, R., & Løset, S. (2015b). In-plane fracture of an ice floe: A theoretical study on the splitting failure mode. *Cold Regions Science and Technology*, *110*, 77 – 101.

Lubbad, R., & Løset, S. (2011). A numerical model for real-time simulation of shipice interaction. *Cold Regions Science and Technology*, *65*.

Lubbad, R., Løset, S., Hedman, U., Holub, C., & Matskevitch, D. (2016). Oden Arctic Technology Research Cruise 2015. In *Arctic Technology Conference*. doi:10.4043/27340-MS.

Lubin, D., & Massom, R. (2006). Polar remote sensing. chapter Sea ice. (pp. 308 – 728). Springer.

Masterson, D. M., Spencer, P. A., Nevel, D. E., & Nordgren, R. P. (1999). Velocity effects from multi-year ice tests. In *18th International Conference on Offshore Mechanics and Arctic Engineering*.

Matusiak, J. (1982). *Dynamic loads and response of icebreaker Sisu during continuous icebreaking*. Technical Report Winter Navigation research board Helsinki.

Matz, G., & Hlawatsch, F. (2003). Wigner distributions (nearly) everywhere: time-frequency analysis of signals, systems, random processes, signal spaces, and frames. *Signal Processing*, *83*, 1355 – 1378.

Ohm, J.-R., & Lüke, H. D. (2010). *Signalübertragung*. Springer.

Riska, K. (2011). Ship-ice interaction in ship design: Theory and practice. In *Encyclopedia of Life Support Systems (EOLSS), Developed under the Auspices of the UNESCO*. Eolss Publisher.

Sodhi, D. S. (1991). Ice - Structure Interaction During Indentation Tests. In *Ice-Structure Interaction* (pp. 619–640). Berlin, Heidelberg: Springer Berlin Heidelberg. doi:10.1007/978-3-642-84100-2_31.

Su, B., Riska, K., & Moan, T. (2010). A numerical method for the prediction of ship performance in level ice. *Cold Regions Science and Technology*, *60*.

Yue, Q., Guo, F., & Krn, T. (2009). Dynamic ice forces of slender vertical structures due to ice crushing. *Cold Regions Science and Technology*, *56*.

Yue, Q., Qu, Y., Bi, X., & Krn, T. (2007). Ice force spectrum on narrow conical structures. *Cold Regions Science and Technology*, *49*, 161 – 169.